Article:
Shirazi, H.A., Chan, C.-W. and Lee, S. (2021) Elastic-plastic properties of titanium and its alloys modified by fibre laser surface nitriding for orthopaedic implant applications. Journal of the Mechanical Behavior of Biomedical Materials, 124. 104802. ISSN: 1751-6161

https://doi.org/10.1016/j.jmbbm.2021.104802

Elastic-plastic properties of titanium and its alloys modified by fibre laser surface nitriding for orthopaedic implant applications

Hadi Asgharzadeh Shirazi,[1] Chi-Wai Chan,[2] Seunghwan Lee[1]
[1]Department of Mechanical Engineering, Technical University of Denmark, Kgs. Lyngby DK-2800 Denmark
[2]Bioengineering Research Group, School of Mechanical and Aerospace Engineering, Queen's University Belfast, BT9 5AH, UK

Abstract

Laser nitriding is one of the most promising approaches to improve wear resistance of Ti alloy surfaces and may extend the use in orthopaedic implants. In this study, three types of Ti alloys, namely alpha commercially pure Ti ("TiG2"), alpha-beta Ti-6Al-4V ("TiG5"), and beta Ti-35.5Nb-7.3Zr-5.7Ta ("βTi"), were subjected to an open-air laser nitriding treatment. Essential elastic-plastic mechanical properties including elastic modulus, hardness, elastic energy, plasticity index, and hardness-to-elasticity ratio of the laser-treated Ti alloys were characterized using nanoindentation experiment. The results showed that the elastic modulus, hardness and elastic energy values of all Ti samples significantly increased in the nitrided layer compared to respective bare substrates for all three Ti materials. Across different Ti samples, βTi sustained its relatively lower elastic modulus, but presented comparable hardness, elastic energy, plasticity index, as well as hardness-to-elasticity ratio in the nitrided layer compared to the other two Ti alloys. Overall, amongst three medical grade Ti alloys in this study, βTi appeared as the most appealing candidate for joint replacement applications even solely in view of mechanical compatibility when combined with surface laser nitriding. Nevertheless, laser nitriding treatment in this study tended to cause a residual compressive stress on all Ti alloys as displayed by cracks developed in the nitrided layer and analyzed on βTi by X-ray diffraction (XRD) and further nanoindentation tests.

Keywords: Fibre laser treatment; Orthopaedic implants; Elastic-plastic properties; Wear ability; Nanoindentation.

1. Introduction

Titanium (Ti) and its alloys, particularly Ti6Al4V (Grade 5), have long been known as a workhorse in bio-implant applications owing to their desirable combination of properties such as biocompatibility, high specific strength to weight ratio, excellent corrosion resistance, modifiable surface properties, high fatigue strength and good toughness [1-4]. In spite of these unique features of Ti and its alloys, they have some critical problems like poor resistance to wear, which prevents the applications for the parts where tribological stress is expected (i.e. contact motions in joint implants). For instance, while Ti6Al4V alloys are widely used for joint replacement prosthesis due to its excellent biocompatibility, they are either not used for bearing parts, e.g.

femoral head-acetabular cup pair because of excessive wear [2,6,7] or need further improvements in femoral head-taper junction because of tribocorrosion [8,9]. Essential to solve this problem is to improve the wear-resistance of Ti surfaces, and a number of different techniques have been devised and applied for this purpose. Representative examples in the techniques include thermal spraying [10,11], physical vapor deposition [12], ion implantation [13], electrical treatments [14,15], chemical vapor deposition [16] to name a few. For more detailed and comprehensive overview on the techniques, readers are directed to a few recent review papers on this topic [2, 4, 16,17].

Among these techniques, laser remelting under nitrogen shielding (or laser nitriding) is one of the most effective surface modification techniques to enhance the surface hardness and wear resistance of Ti alloys by formation of TiN layer on the surface [18-22]. Unlike the TiN coating or layer created by other conventional methods e.g. physical/chemical vapor deposition (P/CVD), the TiN layer formed by open-air laser nitriding provides several advantages such as high speed, cleanliness, short treatment time, high precision, controllable accuracy, reproducibility and elimination of undesirable heating of the substrate thanks to the use of automated fiber laser system [18-22]. Most importantly, in conventional treatment methods, delamination of TiN coating from the substrate has long been a serious concern. Diffusion of high purity N_2 into outermost region of the substrate under high pressure and energy, as well as formation of the deep, hard nitrided-TiN layer (thickness of >50 μm) that metallurgically bonded with the substrate effectively help alleviate the delamination in fibre laser nitriding [19-22]. Notwithstanding these key advantages, only limited studies have been devoted to the improvement of wear and corrosion resistance of Ti alloys via laser gas alloying with nitrogen to date. Chan et al. investigated the effects of laser surface treatment on the antibacterial properties [19], wear and corrosion resistance of commercially pure Ti (Cp Ti, Grade 2), Ti6Al4V (Grade 5) [20] and Ti–Nb–Zr–Ta TNTZ beta Ti [21,22] alloy implant materials. These studies indicated that the laser surface treatment techniques significantly improved not only the wear and corrosion resistance [20-22] but also anti-bacterial adhesion properties on the laser-treated surfaces [19,22]. In order to extend the use of Ti in orthopaedic implants, however, appropriate mechanical properties such as low elastic modulus (close to the human bones), sufficient ductility and high strength, are further required [1]. Thus, the assessment of some relevant and important mechanical properties of laser nitrided Ti alloys is of vital importance to facilitate practical applications.

In this sense, the present study was undertaken to evaluate the mechanical properties of three laser-nitrided Ti alloys, namely alpha Cp Ti (Grade 2), alpha-beta Ti6Al4V (Grade 5) and beta Ti–Nb–Zr–Ta (TNZT) alloys, with an emphasis on characterization of elastic-plastic behavior using nanoindentation measurement. A variety of beta Ti alloys with different properties has been developed by controlling their non-toxic elements (Zr, Nb, Ta, Mo, Fe, etc.) [21-23]. Among various beta Ti biomaterials, the quaternary TNZT alloy was selected as it is one of the most attractive classes owing to its lowest elastic modulus and superb long-term stability against corrosion in biological environments, and is receiving rapidly growing interest in this field

[21,22]. In this sense, a particular focus was placed on the quaternary TNZT beta Ti to further investigate its residual stress induced by laser nitriding on the mechanical reliability and longevity of orthopaedic implant system. The findings of this paper are expected to provide important insights in the field of laser surface nitriding and disclose that this type of surface treatment can play a crucial role in the mechanical aspects of laser-nitrided Ti alloys.

2. Materials and methods

2.1 Materials

Three types of Ti alloys, namely commercially pure (cp) Ti (purity ~99.2%, Grade 2, Zapp Precision Metals GmbH, Germany), Ti6Al4V (Grade 5, Zapp Precision Metals GmbH, Germany), and TNZT β-Ti (Ti-35.5Nb-7.3Zr-5.7Ta, American Element, USA), were used for experiments. Hereafter, the employed Ti samples are denoted as TiG2, TiG5 and βTi, respectively, for convenience. Before laser nitriding, TiG2 and TiG5 were prepared in disc-shapes with dimensions of 30 mm in diameter and 5 mm in thickness. A 40 mm × 30 mm × 3 mm (thickness) rectangular-shaped βTi was also prepared from a larger flat plate. All specimen surfaces were polished by a series of SiC sandpapers from 120 to 800 grit in accordance with standard metallography procedure prior to laser procedure. Next, the specimens were cleaned in ethanol bath for 10 min, rinsed in distilled water, and then blown-dried.

2.2 Fibre laser nitriding treatment

The laser nitriding process was carried out using an automated continues wave (CW) laser system (SPI Lasers UK Ltd, UK). Briefly, after cleaning and drying the samples, they were irradiated with the fibre laser beam with wavelength of 1,070 nm and spot size of 100 μm via an array of pre-set parameters e.g. laser power of 40 W, scanning speed of 25 mm/s and shielding with high purity N_2 at 5 bar in an open-air condition. More detailed parameters with regard to the laser nitriding procedure can be found in recent papers [19-22]. Figure 1 shows a gold-coloured TiN surface created on one of sample; 'dark-bluish' colour on top of the image is possibly indebted from a thicker oxide at the edges of laser-treated area [20].

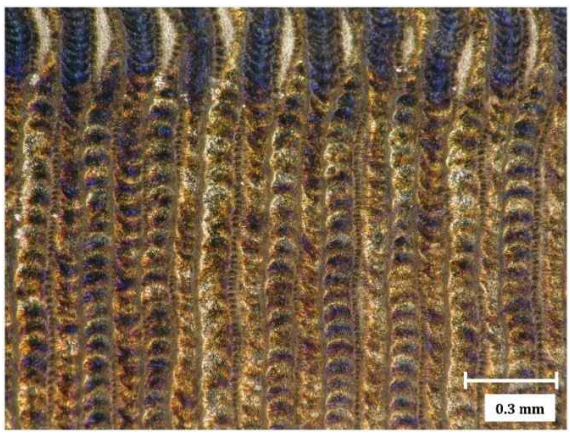

Figure 1. An optical micrograph for the surface of laser-nitrided βTi specimen.

2.3 Sample preparation for nanoindentation tests

In order to investigate the mechanical properties of samples along cross-section, test specimens were cut into two halves perpendicularly through the centerline. Each subsection of samples was initially molded in cross-section view. Afterwards, cross-sectional surfaces were polished with SiC sandpapers in sequence (320, 500, 1000 and 4000) and finally polished using 1 μm and 3 μm diamond suspensions to achieve the smooth surfaces needed for nanoindentation experiments.

2.4 Nanoindentation measurements

Nanoindentation measurements were performed using a Berkovich indenter (CSM Instruments, Peseux, Switzerland), applying a maximum normal load of 50 mN with constant rate of 100 mN·min^{-1}. At least 50 indentations were carried out on each specimen at a room temperature of 23 °C and the averages with standard deviations (SD) of the tests are reported.

During the nanoindentation tests, a high-precision gauge continuously monitors the values of load and displacement. These load-displacement data can deliver a set of important mechanical properties as described below.

2.4.1 Elastic modulus and hardness

Following one cycle of nanoindentation, the load and the displacement of both loading and unloading steps obey power-law relations as follows [24,25]:

$$P = \alpha_1 h^{m1} \qquad \text{In the Loading phase} \qquad (1a)$$

$$P = \alpha\left(h - h_f\right)^m \qquad \text{In the Unloading segment} \qquad (1b)$$

where P and h denote the load and the displacement, respectively; h_f is the depth of residual impression when the indenter is completely removed from the sample (after unloading). α_1, α, m_1 and m are the empirical fitting parameters. In order to obtain the elastic modulus and the hardness of the alloys from nanoindentation tests, the method of Oliver and Pharr was employed [26,27]. In this method, the initial slope of the unloading curve, S, is defined as the contact stiffness and can be calculated as:

$$S = \left[\frac{dP}{dh}\right]_{h=h_m} = \alpha m\left(h_m - h_f\right)^{m-1} \qquad (2)$$

in which h_m is the maximum penetration depth (see Figure 2).

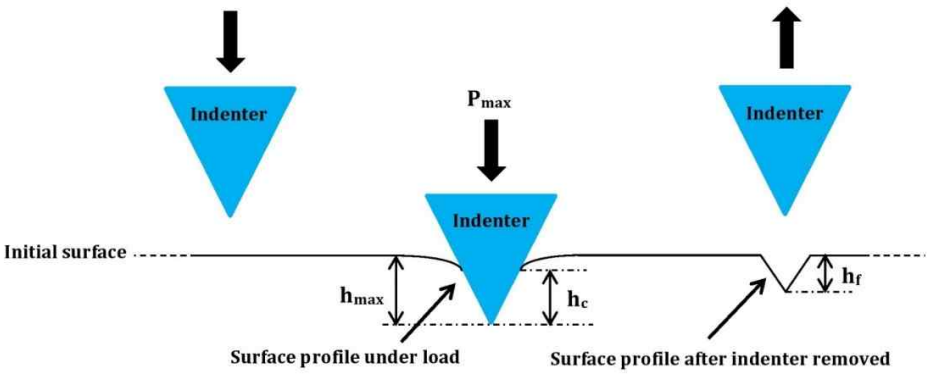

Figure 2. A schematic of the interaction between Berkovich indenter tip and specimen (P_{max}=maximum applied load; h_{max}=maximum depth; h_c=contact depth and h_f=final depth).

The elastic modulus of the test sample can be then calculated based on Sneddon relationship as [24]:

$$\frac{1}{E_r} = \frac{1-\nu^2}{E} + \frac{1-{\nu_i}^2}{E_i} \tag{3}$$

where E and E_i indicate the elastic moduli of the sample and the indenter, respectively; E_r denotes reduced elastic modulus; ν and ν_i represent Poisson's ratio of the sample and the indenter, respectively;

The hardness can be also obtained as:

$$H = \frac{P_{m\,ax}}{A_C} \tag{4}$$

where P_{max} is maximum applied load and A_C denotes the projected area of the indented impression. Details on the relationship in the equations (1) to (3) are found in the references [26-28].

2.4.2 Elastic-plastic behavior and wear resistance

Plasticity index is a key parameter of the material corresponding to its elastic-plastic behavior in response to external stresses and strains. This term can be extracted from load-displacement curve as below [29,30]:

$$Plasticity\ index = \frac{A_1}{A_1 + A_2} \tag{5}$$

Here, A_1 and A_2 indicate the plastic work and elastic energy, respectively. A_1 is equal to the enclosed area between loading and unloading curves and A_2 is the area encompassed by unloading curve. It is worth noting that the term of (A_1+A_2) represents the total mechanical work done by the indenter during nanoindentation.

Besides the plasticity index, the elastic recovery, defined as $A_2/(A_1 + A_2)$, is also an indication of materials energy corresponding to loading. It particularly signifies how much energy is released from the material after being loaded.

In addition to the aforementioned properties, there are two other parameters, namely H/E_r and H^3/E_r^2 that can be addressed to correlate with the anti-wear capabilities of materials. H/E_r represents materials' ability to resist elastic strain to failure and therefore, the higher value may indicate the better wear resistance of a material [30,31]. H^3/E_r^2 (sometimes referred to as yield pressure) [30] indicates the materials' resistance to plastic deformation in loaded contact, and subsequently the higher H^3/E_r^2 ratio reflects the higher resistance to plastic deformation [32].

2.5 X-ray diffraction

The phases of the βTi surfaces were identified by X-ray diffraction (XRD) using Cu Kα radiation (at 0.15406 nm). The residual stresses near the surface region of the laser-nitrided layer were also determined via the well-established XRD "$sin^2\psi$" method [33]. All residual stress measurements were repeated at three different rotation angles (φ) of 0°, 90° and 180° in order to calculate the residual stress tensor. According to the "$sin^2\psi$" method:

$$\varepsilon_{\phi,\psi}^{hkl} = \frac{1+\upsilon}{E}\sigma_{11}sin^2\psi - 2\frac{\upsilon}{E}\sigma_{11} \quad (6a)$$

$$\varepsilon_{\phi,\psi}^{hkl} = \frac{d_{\phi,\psi}^{hkl} - d_0}{d_0} \quad (6b)$$

where $\varepsilon_{\phi,\psi}^{hkl}$ represents lattice strain for one specific hkl plane; E and v are elastic modulus and Poisson's ratio of the crystal at *hkl*, respectively; and d_0 is unstressed d-spacing. If the Eq. (6b) is substituted into Eq. (6a), new form of the d-$sin^2\psi$ formula will be available as:

$$d_{\phi,\psi}^{hkl} = d_0\frac{1+\upsilon}{E}\sigma_{11}sin^2\psi - 2d_0\frac{\upsilon}{E}\sigma_{11} \quad (7)$$

Therefore, taking a linear graph of d versus $sin^2\psi$ into consideration, σ_{11} can be readily obtained from the slope of the line fitted to diffraction data.

3 Results and Discussion

In an effort to have a comprehensive understanding on the elastic-plastic behavior of three types of Ti alloys in orthopaedic implant applications, an array of essential mechanical properties, including hardness (H), elastic modulus (E), elastic energy, and plasticity index of the alloys, was characterized by means of nanoindentation measurements.

3.1 Elasticity and Hardness

As the first step, the load-displacement curves were acquired from three Ti samples along nitrided layer, Heat Affected Zone (HAZ), and bulk substrates, and the mean and SD values of the elastic modulus (E) and the hardness (H) of all three Ti alloys are presented in Figure 3. The full load-displacement curves and representative indentation images are presented in the Supplementary Information as Figure S1 and Figure S2.

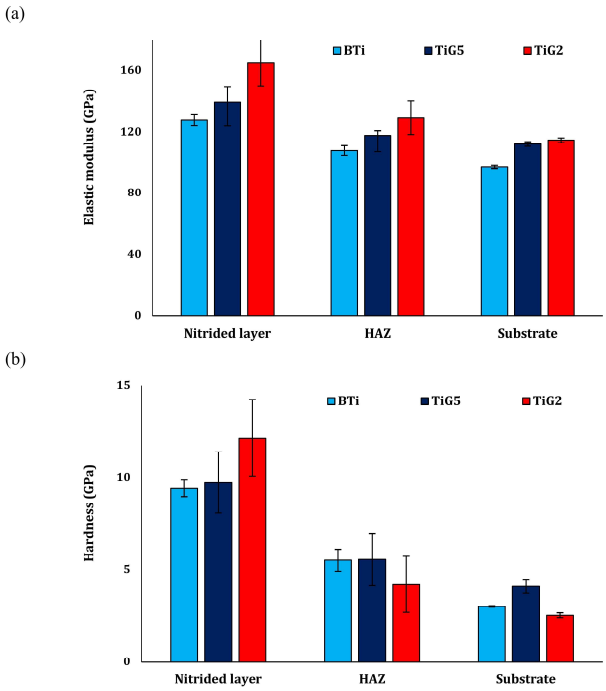

Figure 3. (a) The elastic modulus and (b) the hardness values at three different zones for all used Ti alloys.

As can be clearly seen from this figure, elastic modulus and hardness were in the order of nitrided layer > HAZ > substrate for all three Ti samples. Relative order of the mechanical properties between the Ti samples, however, showed a strong dependence on the region and on whether they being elastic modulus or hardness. For instance, elastic modulus was in the order of TiG2 ≥ TiG5 ≥ βTi in all three regions. Hardness also showed the same trend in the nitrided layer. In contrast, the relative order of hardness in HAZ segment was βTi ≅ TiG5 ≥ TiG2. Moreover, hardness in substrate region was TiG5 > βTi > TiG2. TiG2 and TiG5 exhibited larger elastic modulus values than βTi, probably because of the large percentage of α-phase contained in these samples, and the presence of β-stabilizing elements such as Nb is most likely the first reason for the lower elastic modulus of βTi [1,30,34]. On the other hand, βTi showed higher value of hardness compared to TiG2 in substrate region. This is possibly from the large amount of Nb in βTi compositions; Nb is known to exhibit higher hardness than Ti by ~40% [30]. Further, the elastic modulus and the hardness of nitrided layers depend on mainly two factors, namely the volume fraction and crystallographic orientation of TiN dendrites [20-22,35]. According to our previous studies [4-6], TiG2 showed a higher volume fraction of dendrites than TiG5 and βTi. Additionally, the relatively inhomogeneous distributions of TiN dendrites in the nitrided layer with much larger thicknesses was the main reason of the higher elastic modulus and hardness variation in the nitrided layers of TiG2 and TiG5 in comparison to βTi.

3.2 Elastic energy and plasticity index

The elastic energy and plasticity index, corresponding to elastic and plastic energy dissipations during nanoindentation, are also useful parameters that can gauge the elastic-plastic behavior of biomaterials. The elastic energy indicates how much energy is released from a material after being loaded. In addition, plasticity index often reflects the intrinsic plasticity of a given alloy [36]. Figure 4 displays the elastic energy and plasticity index values of three Ti samples in different zones, namely nitrided, HAZ and bulk substrate.

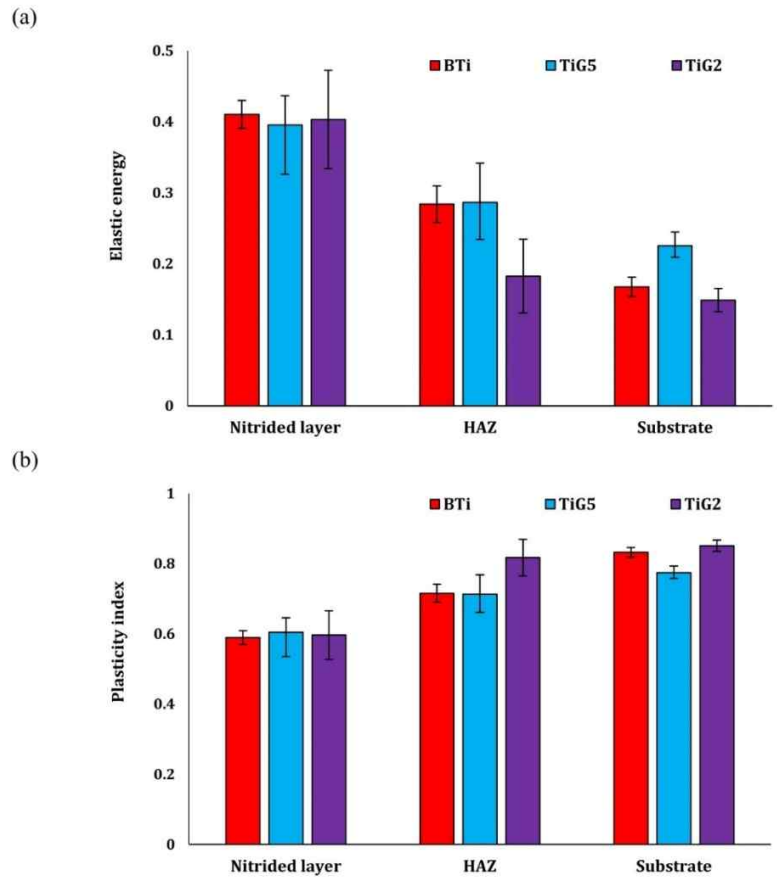

Figure 4. (a) The elastic energy and (b) the plasticity index values of three Ti samples along the nitrided, HAZ, and bulk substrate regions.

As expected, the elastic energy (Figure 4 (a)) was inversely proportional to plasticity index (Figure 4(b)) as it is defined as (1 - *plasticity index*). For all three Ti samples, the elastic energy value was the highest in the nitrided zone, while it decreased upon moving toward HAZ, and then bulk substrate. Accordingly, the plasticity indices were the lowest for the nitrided zone, yet the highest for bulk areas. Across different Ti samples, βTi and TiG2 exhibited higher values of plasticity index than TiG5 in bulk substrate, indicating their larger intrinsic plasticity and hence high ductility and good workability at room temperature compared to TiG5. However, the plasticity index values of all three types of Ti materials in the nitrided layer were statistically

comparable, which indicates that the difference in the plasticity of the top-most layer nearly disappears after laser nitriding. Figure 4 also discloses that laser nitriding resulted in higher resistance to loading, but lesser ductility on the surface nitrided regions of all three Ti alloys. Since typical bio-implants used for bone replacement are not exposed to pronounced plastic strains [36], the reductions in plasticity index in laser-nitrided surface areas are not considered as a serious challenge in orthopaedic field.

3.3 Hardness-to-elasticity ratio, H/E_r and H^3/E_r^2

In addition to elasticity modulus, hardness and elastic energy/plasticity index, the ratio between hardness and elasticity, namely H/E_r, is another mechanical parameter that deserves attention. Recently, H/E_r, together with H^3/E_r^2, has received increasing interest because of its potential relevance to tribological properties, in particular wear resistance [37-40]. Traditionally, hardness has been considered as the primary parameter to explain wear resistance, but it cannot account for that many elastomers with low elasticity modulus also display excellent wear resistance. Several previous studies have reported that H/E_r, or often H^3/E_r^2 as well, are better correlated with wear properties than H alone, especially for some layered materials [37-40]. The values of H/E_r and H^3/E_r^2 for the three Ti samples are presented in Figure 5.

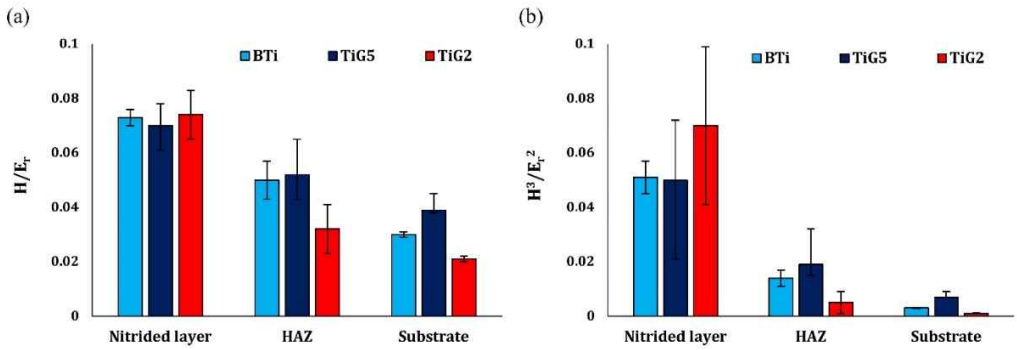

Figure 5. (a) H/E_r and (b) H^3/E_r^2 values of three Ti samples along the nitrided, HAZ, and bulk substrate regions.

According to this figure, the values of H/E_r and H^3/E_r^2 showed the highest values in the nitrided layer and gradually decreased upon shifting to HAZ, and then bulk substrate for all three Ti samples. Meanwhile, the relative order of H/E_r and H^3/E_r^2 across different Ti samples was highly dependent on the region of the samples. Both parameters were close (H/E_r) or statistically similar (H^3/E_r^2), except for TiG2's H^3/E_r^2 where had higher value, in remelted layer for all three samples. TiG2, however, clearly exhibited smaller values for both H/E_r and H^3/E_r^2 compared to βTi and TiG5 in HAZ and base substrates. Between βTi and TiG5, both parameters were comparable to each other in HAZ, but those for TiG5 were distinctively higher than βTi in base substrates. As it is obvious from the figure, the H/E_r and H^3/E_r^2 values increased upon laser nitriding for all three types of Ti samples. This is, in fact, consistent with the significant improvement of wear-resistance of TiG2 [20], TiG5 [20], and two different types of βTi samples

[19, 22] that were observed in previous experimental studies. However, the question of whether the experimental wear properties are better correlated with H/E or H alone across different samples cannot be readily discussed as the experimental conditions for wear properties of different Ti materials were widely different in the previous studies [37-40].

Instead, it is interesting to compare the present study with a similar study by Kümmel et al [40]. In that study, a surface treatment process was carried out to improve the poor tribological properties of Ti6Al4V and the values of hardness, elastic recovery, H/E_r and H^3/E_r^2 were determined by means of nanoindentation. According to their results, the values of hardness, elastic recovery, H/E_r and H^3/E_r^2 were; (i) for near laser-treated surface: 8 GPa, 35%, 0.06 and 0.03; (ii) for bulk: 4 GPa, 20%, 0.03 and 0.004 respectively. The hardness value of HAZ was also measured ~ 4.2 GPa. On the other hand, the present work showed that the values of hardness in three different zones of the laser-treated surface, HAZ and bulk substrate of TiG5 (Ti6Al4V) were determined 9.74 GPa, 5.56 GPa and 4.10 GPa respectively. Comparing our result with Ref. [40], it is obvious that the employed laser treatment in the current paper led to the higher values of hardness in both laser-treated and heat-affected zones. The values of the elastic energy for both laser-treated surface and bulk in our work were about 40% and 22% respectively, where were close to [40]'s elastic recovery outcomes. H/E_r and H^3/E_r^2 values of the present paper were obtained 0.07 and 0.05 for the remelted layer; 0.04 and 0.007 for the bulk substrate, reflecting better anti-wear ability of the laser surface modification process exploited in this work compared to Ref. [40].

Another important subject related to H/E_r is that previous studies have shown that there can be a mathematical relationship between plasticity index and H/E_r in various materials. The relationship has been approximated as following function [41,42]:

$$\text{plasticity index} = 1 - \eta\left(\frac{H}{E_r}\right) \quad (8)$$

The significance of this equation is that there is a universal relationship between the two quantities across different materials and experimental conditions. In order to verify this relationship, the values of plasticity index from the present study were plotted as a function of H/E_r in Figure 5. As expected, a fit of our experimental data confirmed an inversely linear relationship between plasticity index and H/E_r with a slope (η) of ~-5.2 for all three Ti samples. Figure 6 indicates that this relationship is valid not only for different materials, but also for different regions of Ti samples upon laser nitriding.

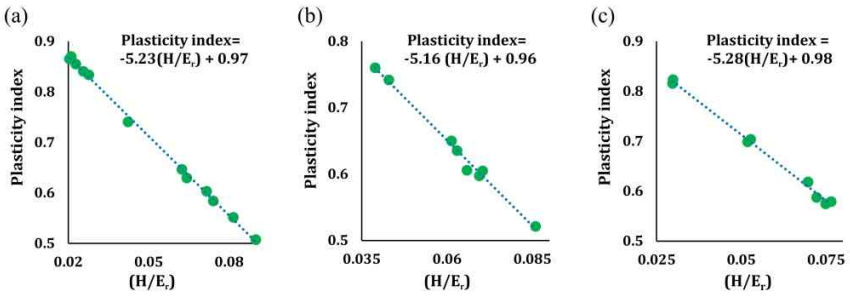

Figure 6. The mathematical relation between plasticity index and H/E_r ratio for three Ti alloys i.e. (a) TiG2, (b) TiG5 and (c) βTi. The lines are a linear fit of the experimental data.

3.4 Residual stress in nitrided zone: a case of βTi

Overall, screening of the fundamental elastic-plastic mechanical properties of the three Ti samples suggests that βTi appears most appealing for orthopaedic implant applications; it is intrinsically lower in elasticity modulus, before and after laser nitriding (Figure 3a), yet comparable in hardness, elastic energy, plasticity index, as well as hardness-to-elasticity ratio compared to the other Ti samples (Figures 3b-5). In addition, TNTZ βTi has no toxic elements that its superior biocompatibility adds more value as bio-implant materials.

Despite the improvement of mechanical properties of Ti materials by laser nitriding, the occurrence of cracks in the nitrided layer remained as an outstanding problem [20]. This was attributed to either too much energy input or too long interaction time in CW of laser nitriding treatment [20]. Even without laser nitriding treatment, cracks were reported in some recent studies on other types of βTi too [43,44]. In coatings, residual stress is another parameter that has a critical influence on the mechanical properties of materials e.g. elastic-plastic behavior, fatigue, fracture, corrosion and wear [45-47]. The cross-sectional micrographs for all three laser-nitrided Ti alloys are depicted in Figure 7.

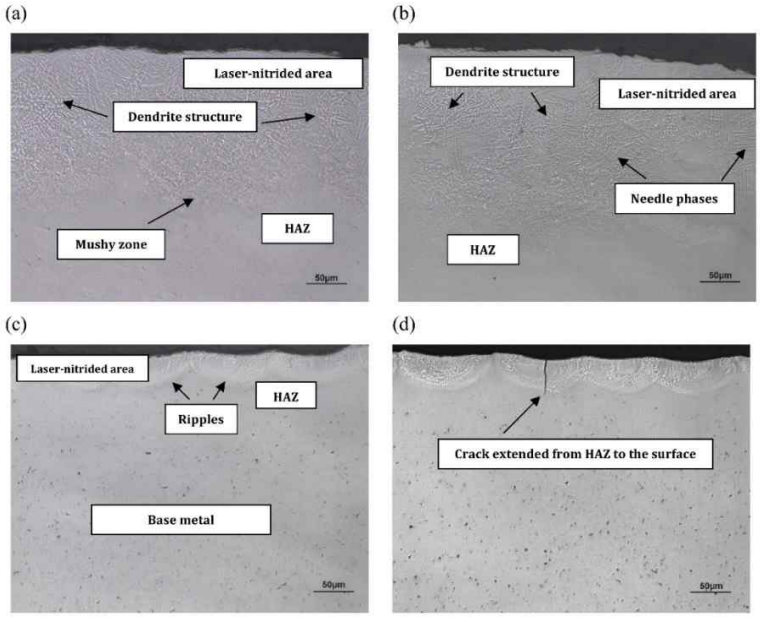

Figure 7. The cross-sectional microscope images for laser-nitrided (a) TiG2, (b) TiG5 and (c) βTi alloys; (d) the presence of perpendicular crack in nitrided layer of βTi sample. It should be noted that cracks were observed from all three Ti samples, and the one in (d) is chosen only as an example.

As can be seen from Figure 7d, crack appeared on the Ti sample surfaces after laser nitriding (e.g. a few cracks across the whole of βTi laser-nitrided layer can be observed). Similar cracks were observed in the laser-nitrided surfaces of both TiG2 and TiG5 too (data not shown). There are mainly two possibilities for the formation of the cracks [48]; firstly, if the semi-brittle layer is subjected to excessively high lateral tensile residual stresses, it may relax itself by forming tensile cracks perpendicular to the interface. Secondly, if the layer is exposed to critically high compressive stresses, relaxation can take place by creation of a regular pattern of shear cracks. The residual stresses of thin layers may be normally variable in the range of 0.1–3 GPa in compression, and up to 1 GPa in tension [48]. Figure 7 shows that the cracks were developed perpendicularly from the boundary of TiN and bulk zones to the sample surface. Considering the direction of stress and resultant strain, it is reasonable to propose that the residual stress in the nitrided layers is predominantly tensile stress.

As βTi is the most attractive Ti material as bio-implant applications as given above, we have selected βTi as the sample to perform XRD to verify the hypothesis on residual stress. The measurement relies on the shifts in the position of the diffraction peaks when the specimen is tilted by angle of ψ in a specific φ angle. Thus, the magnitude of the peak shift, if it occurs at all, corresponds to the magnitude of structural change, and in turn, the residual stress according to Eq. (7). If there are no shear strains in the surface region of specimen, the d spacing would change linearly with $sin^2\psi$. Figure 8 demonstrates the d spacing measurement as a function of $sin^2\psi$ for the nitrided layer of βTi alloy accompanied by the XRD patterns on the TiN (2 2 0) and

Ti β-phase (2 2 0) with different inclination angles for three φ angles i.e. 0°, 90° and 180°. The linear behavior of d-$sin^2\psi$ (Figure 8(b-c)) indicates a homogeneous stress. Moreover, the positive slope in this plot reflects that the residual stress in the nitrided layer is tensile. Shifting the central peak of the XRD pattern of βTi specimen with different inclination angles to the right direction further supports that the observed tensile residual stress in the nitrided layer.

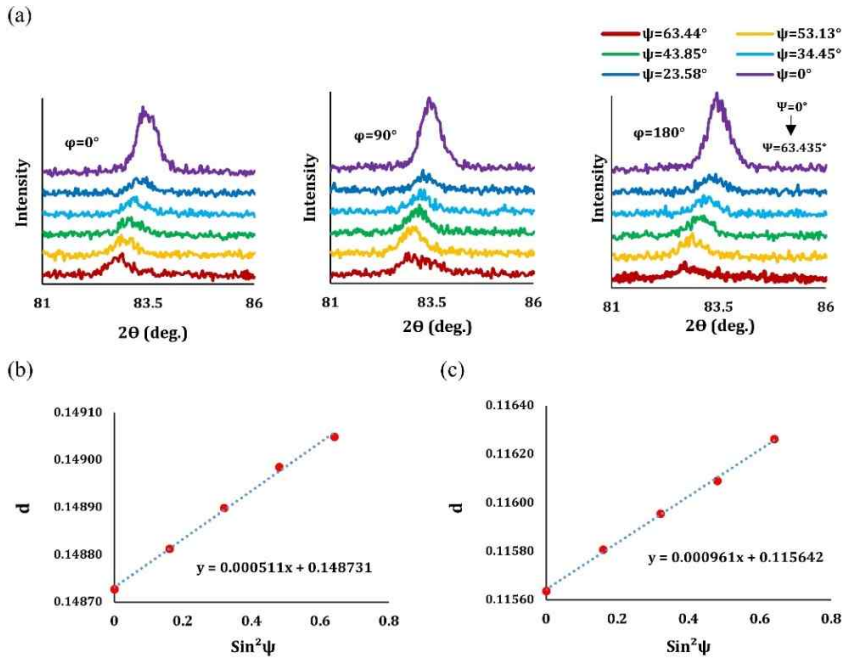

Figure 8. (a) The XRD pattern on the B-Ti (2 0 0) plane of βTi specimen with different inclination angles; and the plots of d versus $sin^2\psi$ for (b) TiN (2 2 0) at 2Θ ~62°and (c) β-Ti (2 0 0) at 2Θ ~82° for βTi specimen.

The calculations were carried out by tracking two TiN peaks (2 2 0) at 2Θ ~62°, and the Ti β-phase (2 2 0) at 2Θ ~82°. These peaks were opted based on the XRD profile of both untreated and treated βTi parts with well-identified peaks shown in Figure 8.

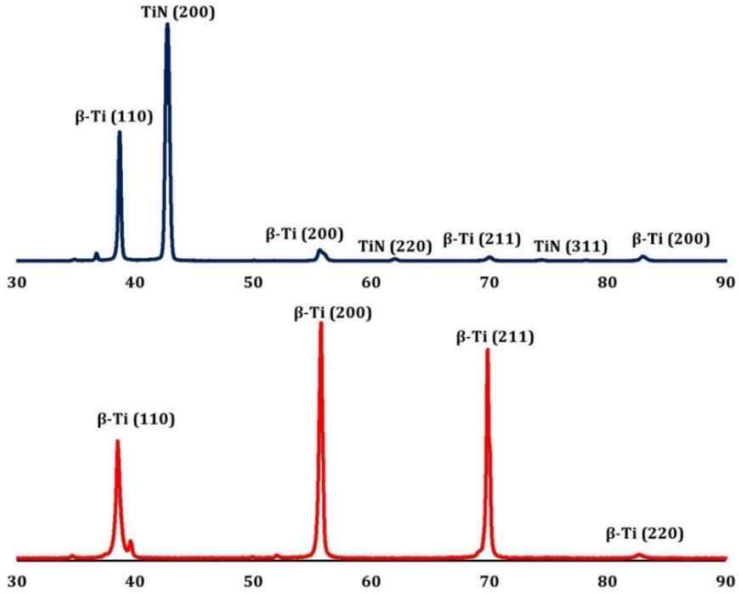

Figure 9. The XRD patterns obtained from laser treated and untreated zones of BTi alloy.

It was attempted to select the peaks of TiN and Ti with high 2Θ as well as isolated peaks in the specific range to prevent misunderstanding with neighbor peaks after being shifted. For both, the residual stresses were equal to 507.3 ± 48.0 MPa (for TiN peak) and 695.9 ± 27.0 MPa (for Ti peak).

Previous researches in literature revealed that the mechanical properties of materials, including elastic modulus, hardness and load-displacement curve of thin layers, could be influenced by different types of residual stresses [45-47]. To elucidate the affecting extent of residual stresses on the experimental data measured by nanoindentation test, a zigzag pattern was chosen from the surface of laser treated βTi to the position far away from HAZ-bulk boundary placed in the bulk zone. Figure 9 manifests load-displacement curves, elastic modulus and hardness values in the different laser-nitrided regions of βTi in accordance to chosen zigzag pattern.

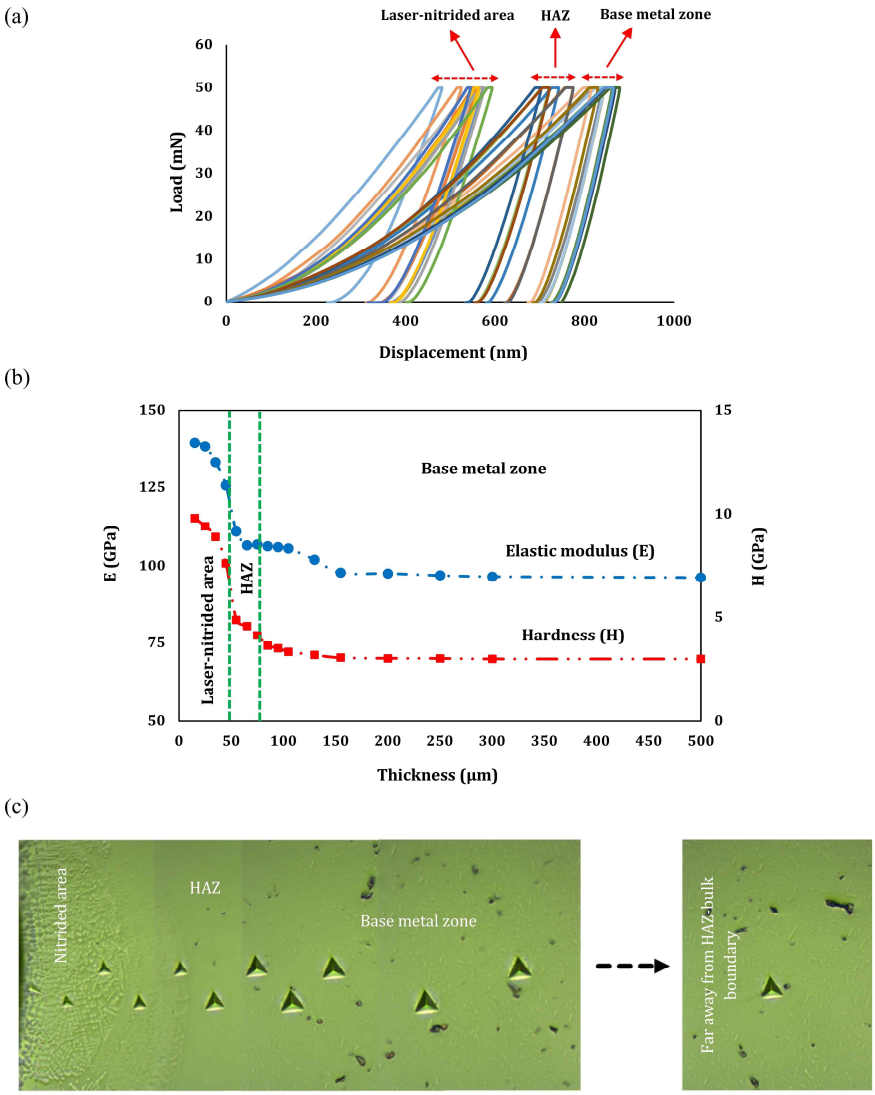

Figure 10. (a) Load-displacement curves and (b) *E* and *H* trends vs. depth caused by indenting from the nitrided zone to bulk substrate of βTi alloy; (c) the optical micrograph of a residual indentation at three different areas of laser-nitrided βTi.

As shown in this figure, the elastic modulus and hardness display a decreasing trend from the nitrided region to the base metal substrate. In particular, the elastic modulus and hardness in the nitrided region were much higher than those in the bulk substrate. The increases in the elastic modulus and the hardness directly enhance the stiffness and the wear resistance of material components, which will be further discussed below. Figure 10a was also an obvious proof on the improvement of stiffness and the strength of βTi alloy modified by nitriding laser treatment. However, focusing on the substrate region (bulk zone in Figure 10b), it is noticeable that the values of elastic modulus and hardness kept reducing as well as that load-displacement kept

shifting to right (higher depth value) even in this region alone, before they reached the stable status. We propose that this trend may be ascribed to the existence of the residual compressive stress in substrate generated after laser nitriding. As a counter-action of generating the residual tensile stress in the nitrided zone, the structure (bonding atoms) at HAZ-bulk boundary can be rather compressed, and as a result, the indenter could penetrate less into this part compared to the zone far away from the boundary in the bulk in which the intensity of residual stress decreased. In other words, laser nitriding treatment appears to have caused a residual compressive stress on the βTi substrate; however, further technical investigations in this field are necessary to verify such assumptions. This is critically important because one of the main factors leading to mechanical damages is residual stresses, playing a significant role in the mechanical performance and reliability of material covered by thin layer [46,47].

Conclusion

The improvement of wear resistance by laser-nitriding treatment has been verified in many recent studies [3-7]. However, concomitant changes in mechanical properties upon laser nitriding have been less studied and understood to date. In this study, the elastic-plastic behaviors of laser-nitrided Ti samples were characterized and compared by employing Cp Ti (TiG2), Ti6Al4V (TiG5) and 35.5Nb-7.3Zr-5.7Ta βTi alloy. The conclusions drawn from this study include;

1. For all three types of Ti samples, the elastic modulus, hardness and elastic energy values significantly increased in the nitrided layer, followed by HAZ compared to bulk substrate.

2. Accordingly, the plasticity indices indicated less ductility on the surface nitrided regions of the three Ti alloys after laser nitriding.

3. Among the three types of Ti materials studied, βTi appeared the most appealing choice for joint replacement applications due to the higher mechanical compatibility (e.g. lower elastic modulus) and yet comparable in terms of hardness, elastic energy, plasticity, and hardness-to-elasticity ratios compared to TiG2 and TiG5. Absence of toxic elements in 35.5Nb-7.3Zr-5.7Ta βTi alloy is additional merit for this material as bio-implant material.

4. Nevertheless, cracks developed in the nitrided layer after laser nitriding treatment in this study is an outstanding problem. Investigation by X-ray diffraction (XRD) and further nanoindentation tests on βTi sample suggests that a residual compressive stress might be responsible for the cracks.

References

[1] Brunette DM, Tengvall P, Textor M, Thomsen P, editors. Titanium in medicine: material science, surface science, engineering, biological responses and medical applications. Springer Science & Business Media; 2012 Dec 6.

[2] Seifalian A, de Mel A, Kalaskar DM, Kulkarni M, Mazare A, Schmuki P, Iglič A. Chapter 5. Biomaterial surface modification of titanium and titanium alloys for medical applications. In book: Nanomedicine. 2014. pp.111-136. One Central Press.

[3] Zhang LC, Chen LY. A review on biomedical titanium alloys: Recent progress and prospect. Advanced Engineering Materials. 2019 Mar;21;1801215.

[4] Liu W, Liu S., Wang L. Surface modification of biomedical titanium alloy: Micromorphology, microstructure evolution and biomedical applications. Coatings. 2019 Apr;9(4):249.

[5] Cordova LA, Stresing V, Gobin B, Rosset P, Passuti N, Gouin F, Trichet V, Layrolle P, Heymann D. Orthopaedic implant failure: aseptic implant loosening–the contribution and future challenges of mouse models in translational research. Clinical Science. 2014 Sep 1;127(5):277-93.

[6] Merola M, Affatato S. Materials for hip prostheses: A review of wear and loading considerations. Materials. 2019 Feb;12(3): 495.

[7] Drummond J, Tran P, Fary C. Metal-on-metal hip arthroplasty: A review of adverse reactions and patient management. Journal of Functional Biomaterials. 2015 Sep;6(3): 486–499.

[8] Hussenbocus S, Kosuge D, Solomon LB, Howie DW, Oskouei RH. BioMed Research International. 2015 Mar;2015:758123.

[9] Stockhausen KE, Riedel C, Belinski AV, Rothe D, Gehrke T, Klebig F, Gebauer M, Amling M, Citak M, Busse B. Variability in stem taper surface topography affects the degree of corrosion and fretting in total hip arthroplasty. Scientific Reports. 2021;11:9348.

[10] Singh H, Sidhu BS, Puri D, Prakash S. Use of plasma spray technology for deposition of high temperature oxidation/corrosion resistant coatings – A review. Materials and Corrosion. 2007 Jan;58: 92.

[11] Bhadang KA, Holding CA, Thissen H, McLean KM, Forsythe JS, Haynes DR. Biological responses of human osteoblasts and osteoclasts to flame-sprayed coatings of hydroxyapatite and fluorapatite blends. Acta Biomaterialia. 2010 Apr;6(4):1575-1583.

[12] Mao D, Hopwood J. Ionized physical vapor deposition of titanium nitride: A deposition model. Journal of Applied Physics. 2004 Jun;96:820.

[13] Rautray TR, Narayanan R, Kwon TY, Kim KH. Surface modification of titanium and titanium alloys by ion implantation. Journal of Biomedical Materials Research Part B: Applied Biomaterials. 2010 May; 93(2):581-591.

[14] M. Köunönen, M. Hormia, J. Kivilahti, J. Hautaniemi, I. Thesleff, Effect of surface processing on the attachment, orientation, and proliferation of human gingival fibroblasts on titanium. Journal of Biomed Materials Research. 1992 Oct; 26:1325.

[15] Larsson C, Thomsen P, Aronsson BO, Rodahl M, Lausmaa J, Kasemo B, Ericson LE. Bone response to surface-modified titanium implants: studies on the early tissue response to machined and electropolished implants with different oxide thicknesses. Biomaterials 1996 Mar;17(6): 605-616.
[16] Giavaresi G, Giardino R, Ambrosio L, Battiston G, Gerbasi P, Fini M, Rimondini L, Torricelli P. In vitro biocompatibility of titanium oxide for prosthetic devices nanostructured by low pressure metal-organic chemical vapor deposition. International Journal of Artificial Organs. 2003;26:774–780.
[17] Zhang LC, Chen LY, Wang L. Surface modification of titanium and titanium alloys: Technologies, developments, and future interests. Advanced Engineering Materials. 2020;22: 1901258.
[18] Tian YS, Chen CZ, Li ST, Huo QH. Research progress on laser surface modification of titanium alloys. Applied Surface Science. 2005 Mar 31;242(1-2):177-84.
[19] Chan CW, Carson L, Smith GC, Morelli A, Lee S. Enhancing the antibacterial performance of orthopaedic implant materials by fibre laser surface engineering. Applied Surface Science. 2017 May 15;404:67-81.
[20] Chan CW, Lee S, Smith GC, Donaghy C. Fibre laser nitriding of titanium and its alloy in open atmosphere for orthopaedic implant applications: Investigations on surface quality, microstructure and tribological properties. Surface and Coatings Technology. 2017 Jan 15;309:628-40.
[21] Chan CW, Lee S, Smith G, Sarri G, Ng CH, Sharba A, Man HC. Enhancement of wear and corrosion resistance of beta titanium alloy by laser gas alloying with nitrogen. Applied Surface Science. 2016 Mar 30;367:80-90.
[22] Chang X, Smith GC, Quinn J, Carson L, Chan CW, Lee S. Optimization of anti-wear and anti-bacterial properties of beta TiNb alloy via controlling duty cycle in open-air laser nitriding. Journal of the Mechanical Behavior of Biomedical Materials. 2020 Oct 1;110:103913.
[23] Guillemot F. Recent advances in the design of titanium alloys for orthopedic applications. Expert review of medical devices. 2005 Nov 1;2(6):741-8.
[24] Sneddon IN. The relation between load and penetration in the axisymmetric Boussinesq problem for a punch of arbitrary profile. International journal of engineering science. 1965 May 1;3(1):47-57.
[25] Doerner MF, Nix WD. A method for interpreting the data from depth-sensing indentation instruments. Journal of Materials research. 1986 Aug;1(4):601-9.
[26] Oliver WC, Pharr GM. An improved technique for determining hardness and elastic modulus using load and displacement sensing indentation experiments. Journal of materials research. 1992 Jun;7(6):1564-83.
[27] Oliver WC, Pharr GM. Measurement of hardness and elastic modulus by instrumented indentation: Advances in understanding and refinements to methodology. Journal of materials research. 2004 Jan;19(1):3-20.
[28] Fischer-Cripps AC. Nanoindentation Springer. New York. 2004.

[29] Bao YW, Wang W, Zhou YC. Investigation of the relationship between elastic modulus and hardness based on depth-sensing indentation measurements. Acta Materialia. 2004 Oct 18;52(18):5397-404.
[30] Hynowska A, Pellicer E, Fornell J, González S, van Steenberge N, Suriñach S, Gebert A, Calin M, Eckert J, Baró MD, Sort J. Nanostructured β-phase Ti–31.0 Fe–9.0 Sn and sub-μm structured Ti–39.3 Nb–13.3 Zr–10.7 Ta alloys for biomedical applications: Microstructure benefits on the mechanical and corrosion performances. Materials Science and Engineering: C. 2012 Dec 1;32(8):2418-25.
[31] Medeiros BB, Medeiros MM, Fornell J, Sort J, Baró MD, Junior AJ. Nanoindentation response of Cu–Ti based metallic glasses: Comparison between as-cast, relaxed and devitrified states. Journal of Non-Crystalline Solids. 2015 Oct 1;425:103-9.
[32] Musil J, Kunc F, Zeman H, Polakova H. Relationships between hardness, Young's modulus and elastic recovery in hard nanocomposite coatings. Surface and Coatings Technology. 2002 May 15;154(2-3):304-13.
[33] Matejicek J, Sampath S, Dubsky J. X-ray residual stress measurement in metallic and ceramic plasma sprayed coatings. Journal of thermal spray technology. 1998 Dec 1;7(4):489-96.
[34] Long M, Rack HJ. Titanium alloys in total joint replacement—a materials science perspective. Biomaterials. 1998 Sep 1;19(18):1621-39.
[35] Vora HD, Rajamure RS, Dahotre SN, Ho YH, Banerjee R, Dahotre NB. Integrated experimental and theoretical approach for corrosion and wear evaluation of laser surface nitrided, Ti–6Al–4V biomaterial in physiological solution. journal of the mechanical behavior of biomedical materials. 2014 Sep 1;37:153-64.
[36] Milman YV. Plasticity characteristic obtained by indentation. Journal of Physics D: Applied Physics. 2008 Mar 12;41(7):074013.
[37] Regent F, Musil J. Magnetron sputtered Cr-Ni-N and Ti-Mo-N films: Comparison of mechanical properties. Surface and Coatings Technology. 2001 Jul;142-144:146-151.
[38] Musil J, Kunc F, Zeman H, Poláková H. Relationships between hardness, Young's modulus and elastic recovery in hard nanocomposite coatings. Surface and Coatings Technology. 2002 May;154(2–3):304-313.
[39] Leyland A, Matthews A. On the significance of the H/E ratio in wear control: A nanocomposite coating approach to optimised tribological behavior. Wear. 2000 Nov;246:1–11.
[40] Kümmel D, Linsler D, Schneider R, Schneider J. Surface engineering of a titanium alloy for tribological applications by nanosecond-pulsed laser. Tribology International. 2020 Oct;150:106376.
[41] Cheng YT, Cheng CM. Relationships between hardness, elastic modulus, and the work of indentation. Applied physics letters. 1998 Aug 3;73(5):614-6.
[42] Pellicer E, Pané S, Sivaraman KM, Ergeneman O, Suriñach S, Baró MD, Nelson BJ, Sort J. Effects of the anion in glycine-containing electrolytes on the mechanical properties of electrodeposited Co–Ni films. Materials Chemistry and Physics. 2011 Nov 1;130(3):1380-6.

[43] Rabadia CD, Liu YJ, Cao GH, Li YH, Zhang CW, Sercomb TB, Sun H, Zhang LC. High-strength β stabilized Ti-Nb-Fe-Cr alloys with large plasticity. Materials Science & Engineering A. 2018 Aug;732:368-377.
[44] Rabadia CD, Liu YJ, Jawed SF, Wang LQ, Sun H, Zhang LC. Deformation and toughness behavior of β -type titanium alloys comprising C15-type Laves phase. Materials Today Sustainability.2020 Sep;9:100034.
[45] Qasmi M, Delobelle P, Richard F, Bosseboeuf A. Effect of the residual stress on the determination through nanoindentation technique of the Young's modulus of W thin film deposit on SiO2/Si substrate. Surface and coatings technology. 2006 Apr 10;200(14-15):4185-94.
[46] Huang YC, Chang SY, Chang CH. Effect of residual stresses on mechanical properties and interface adhesion strength of SiN thin films. Thin Solid Films. 2009 Jul 1;517(17):4857-61.
[47] Chen Q, Mao WG, Zhou YC, Lu C. Effect of Young's modulus evolution on residual stress measurement of thermal barrier coatings by X-ray diffraction. Applied Surface Science. 2010 Sep 15;256(23):7311-5.
[48] Holmberg K, Ronkainen H, Laukkanen A, Wallin K, Hogmark S, Jacobson S, Wiklund U, Souza RM, Ståhle P. Residual stresses in TiN, DLC and MoS2 coated surfaces with regard to their tribological fracture behaviour. Wear. 2009 Dec 1;267(12):2142-56.

Supplementary Information for

Elastic-plastic properties of titanium and its alloys modified by fibre laser surface nitriding for orthopaedic implant applications

Hadi Asgharzadeh Shirazi,[1] Chi-Wai Chan,[2] Seunghwan Lee[1]
[1]Department of Mechanical Engineering, Technical University of Denmark, Kgs. Lyngby DK-2800 Denmark
[2]Bioengineering Research Group, School of Mechanical and Aerospace Engineering, Queen's University Belfast, BT9 5AH, UK

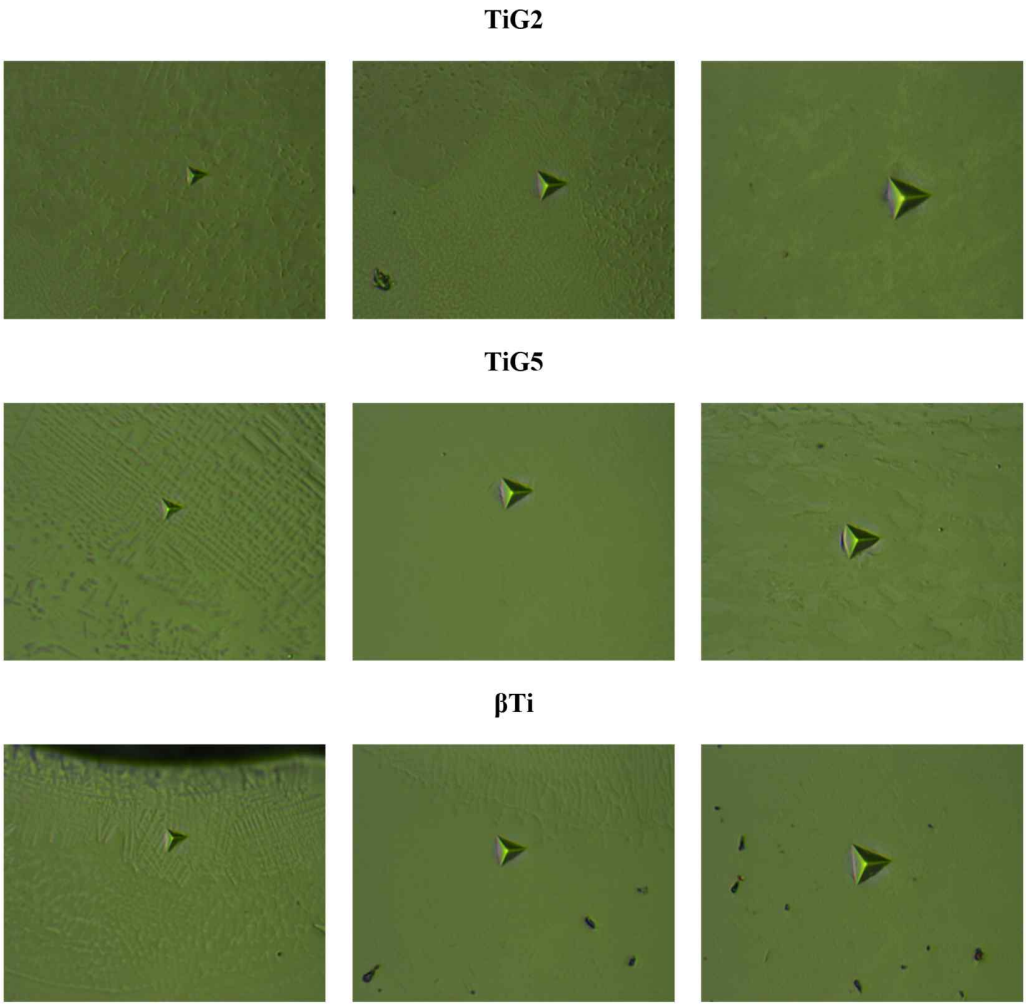

Figure S1. Representative indentation images of three Ti samples

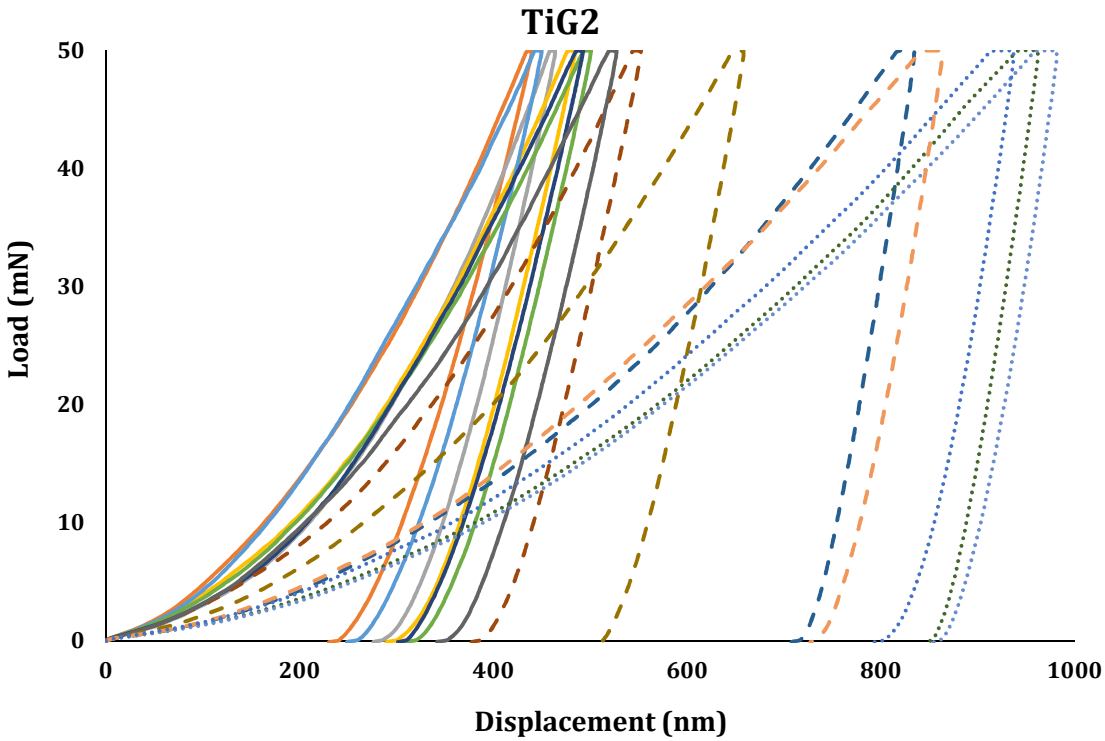
TiG2
Load (mN)
50
40
30
20
10
0
0
200
400
600
800
1000
Displacement (nm)

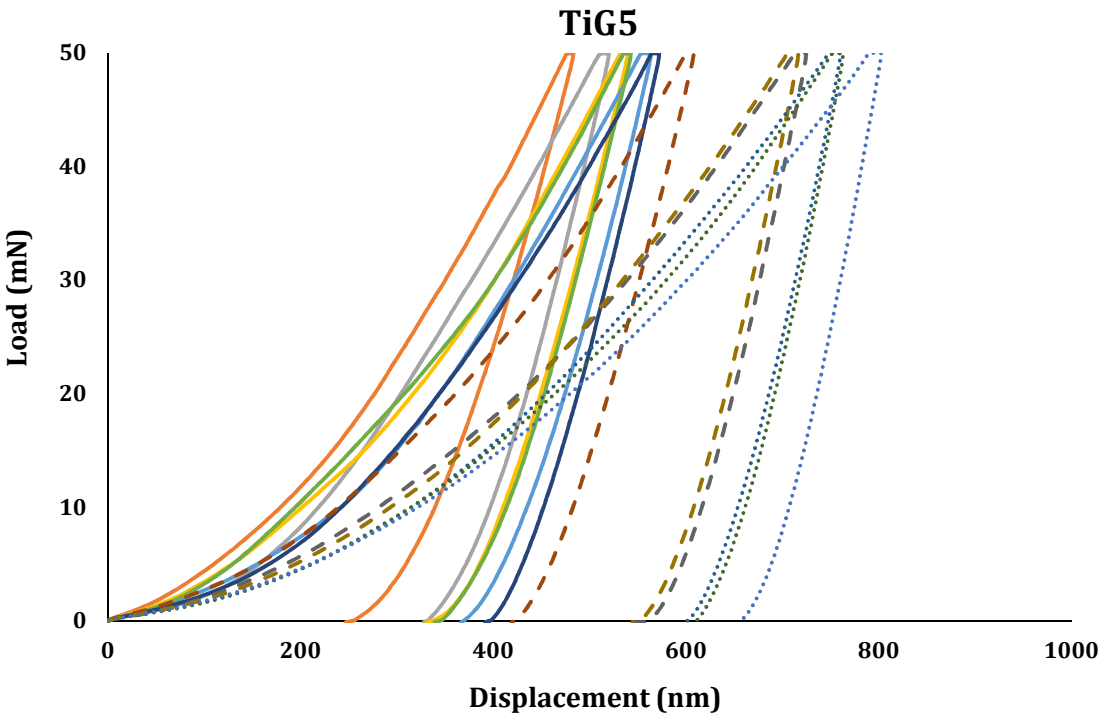
TiG5
Load (mN)
50
40
30
20
10
0
0
200
400
600
800
1000
Displacement (nm)

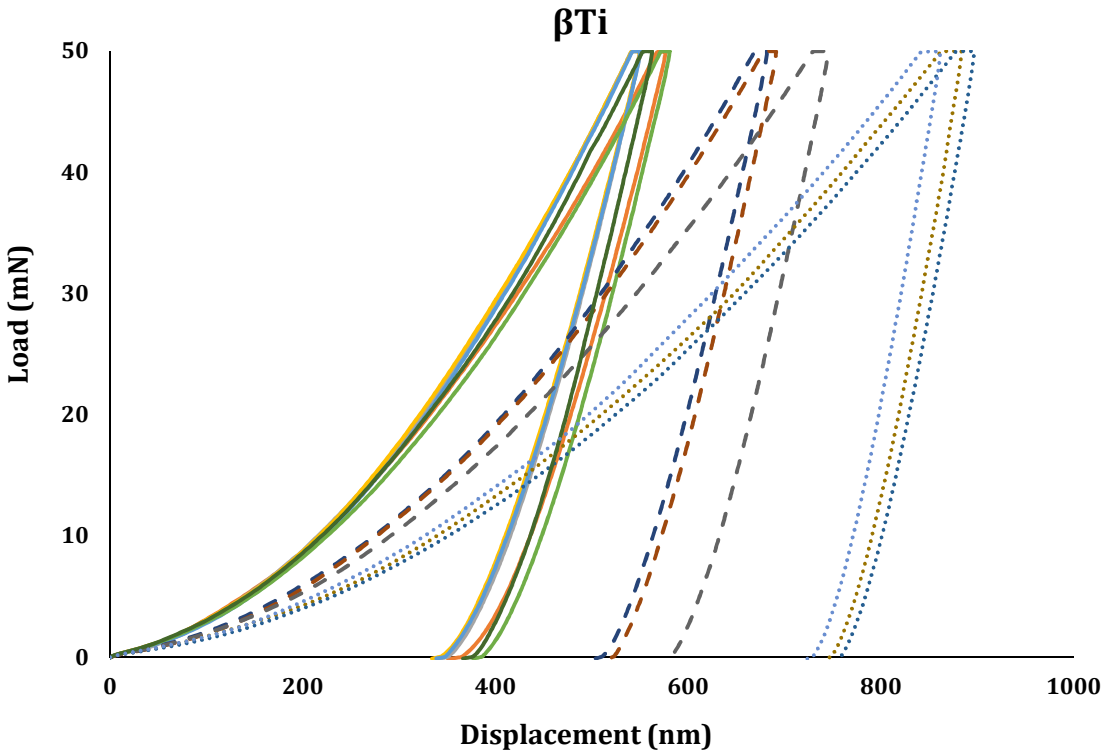

Figure S2. Load-displacement curves for all three laser-treated Ti alloys in the three different zones of (— solid-line) laser-nitrided, (----- dash-line) HAZ, and (….. dot-line) bulk substrate.